

# Flow and Transport in Regions with Aquatic Vegetation

Heidi M. Nepf

Department of Civil and Environmental Engineering, Massachusetts Institute of Technology,  
Cambridge, Massachusetts 02139; email: hmnepf@mit.edu

Annu. Rev. Fluid Mech. 2012. 44:123–42

First published online as a Review in Advance on  
September 9, 2011

The *Annual Review of Fluid Mechanics* is online at  
fluid.annualreviews.org

This article's doi:  
10.1146/annurev-fluid-120710-101048

Copyright © 2012 by Annual Reviews.  
All rights reserved

0066-4189/12/0115-0123\$20.00

## Keywords

canopy, canopy shear layer, monami, turbulence, turbulent transport

## Abstract

This review describes mean and turbulent flow and mass transport in the presence of aquatic vegetation. Within emergent canopies, the turbulent length scales are set by the stem diameter and spacing, and the mean flow is determined by the distribution of the canopy frontal area. Near sparse submerged canopies, the bed roughness and near-bed turbulence are enhanced, but the velocity profile remains logarithmic. For dense submerged canopies, the drag discontinuity at the top of the canopy generates a shear layer, which contains canopy-scale vortices that control the exchange of mass and momentum between the canopy and the overflow. The canopy-scale vortices penetrate a finite distance into the canopy,  $\delta_e$ , set by the canopy drag. This length scale segregates the canopy into two regions: The upper canopy experiences energetic turbulent transport, controlled by canopy-scale vortices, whereas the lower canopy experiences diminished transport, associated with the smaller stem-scale turbulence. The canopy-scale vortices induce a waving motion in flexible blades, called a monami.

## INTRODUCTION

Fresh- and saltwater vegetation provide a wide range of ecosystem services. Seagrasses are essential primary producers, forming the foundation for many food webs (Green & Short 2003). Seagrass meadows also damp waves, stabilize the seabed, shelter economically important fish, and enhance local water quality by filtering nutrients from the water. Based on nutrient cycling services alone, the global economic value of seagrass was estimated to be 3.8 trillion dollars per year by Costanza et al. (1997). Aquatic vegetation is also abundant in lowland rivers, where it provides habitat, alters light availability and temperature, and mediates concentrations of oxygen, carbon, and nutrients (Carpenter & Lodge 1986). Fresh- and saltwater wetlands provide habitat, improve water quality, and reduce coastal erosion (Mitsch & Gosselink 1986, Brampton 1992). Most of the services mentioned above are influenced by the flow within the vegetated regions.

The presence of vegetation alters the velocity field across several scales, ranging from individual branches and blades on a single plant to the community of plants, called the meadow or canopy. The flow structure at the different scales is relevant to different processes. For example, the uptake of nutrients by an individual blade depends on the boundary layer on that blade, i.e., on the blade-scale flow (e.g., Koch 1994, Hurd 2000). Similarly, the capture of pollen is mediated by the flow structure generated around individual stigma (e.g., Ackerman 1997, 2000). In contrast, the flushing of larvae and pollen from a seagrass meadow or kelp forest depends on the flow structure at the canopy scale (e.g., Jackson & Winant 1983, Gaylord et al. 2004).

Some aspects of canopy flow have been described in recent reviews. Monismith (2007) described flow at branch and canopy scales in and around coral. Canopy-scale flow structure for terrestrial plant and urban canopies has been described by Finnigan (2000) and Belcher et al. (2012), and the mechanical interactions between wind and terrestrial plants were described by de Langre (2008). To complement this rich literature, this review emphasizes conditions unique to aquatic vegetation. Specifically, unlike terrestrial canopies, aquatic canopies can occupy all or a large fraction of the flow depth such that the dynamic impact of the canopy is felt over the entire flow domain. This review focuses on the fully developed flow structure over and through long canopies. The adjustment of flow at the leading edge of a canopy has been described by Belcher et al. (2003, 2012) and Rominger & Nepf (2011).

## GEOMETRIC SCALES AND MOMENTUM BALANCE

The canopy geometry is defined by the scale of individual stems and blades and the number of these elements per bed area. If the canopy elements have a characteristic diameter or width,  $d$ , and the average spacing between elements is  $\Delta S$ , then the frontal area per canopy volume is  $\bar{a} = d/\Delta S^2$ . In terrestrial canopy literature, this is called the leaf area index (e.g., Kaimal & Finnigan 1994, p. 79). A nondimensional measure of the canopy density is the frontal area per bed area,  $\lambda_f$ , known as the roughness density (Wooding et al. 1973). For canopy height  $b$ , and  $z = 0$  at the bed,

$$\lambda_f = \int_{z=0}^b a dz = ab, \quad (1)$$

with the right-most expression valid for vertically uniform  $a$ . The canopy density can also be described by the solid volume fraction occupied by the canopy elements,  $\phi$ . If the individual elements approximate a circular cylinder, e.g., reed stems, then  $\phi \approx (\pi/4) ad$ . If the morphology is strap-like, e.g., seagrasses, with blade width  $d$  and thickness  $b$ , then  $\phi = db/\Delta S^2 = ab$ .

Aquatic canopies exhibit a wide range of geometry. Marsh grasses are relatively sparse with  $d = 0.1$  to  $1$  cm,  $\phi = 0.001$  to  $0.01$ , and  $a = 0.01$  to  $0.07$  cm<sup>-1</sup> (based on Valiela et al. 1978; Leonard & Luther 1995, Lightbody & Nepf 2006). Mangroves are among the densest canopies,

with  $\phi$  as high as 0.45, mean trunk diameters of 4 to 9 cm, and  $a$  up to  $0.2 \text{ cm}^{-1}$  (Mazda et al. 1997, Furukawa et al. 1997). Seagrasses have  $a = 0.01$  to  $1 \text{ cm}^{-1}$  and  $\phi = 0.01$  to 0.1 (Chandler et al. 1996, Luhar et al. 2010). Emergent plants tend to have rounded stems for higher stiffness, and submerged grasses tend to have a blade geometry in which the width (0.3 to 1 cm) is larger than the thickness ( $\approx 0.1 \text{ cm}$ ), in which case  $d$  is the blade width.

Within a canopy, flow is forced to move around each branch or blade so that the velocity field is spatially heterogeneous at the scale of these elements. A double-averaging method is used to remove the element-scale spatial heterogeneity, in addition to the more common temporal averaging (Gray & Lee 1977; Raupach & Shaw 1982, and references therein). We let the coordinates  $x$  and  $z$  be parallel and normal to the local mean bed slope, with  $z = 0$  at the bed and positive away from the bed. The velocity vector  $\vec{u} = (u, v, w)$  corresponds to the coordinates  $(x, y, z)$ , respectively. The instantaneous velocity and pressure ( $p$ ) fields are first decomposed into a time average (overbar) and deviations from the time average (single prime). The time-averaged quantities are further decomposed into a spatial mean (angle bracket) and deviations from the spatial mean (double prime). The spatial averaging volume is thin in the vertical direction, to preserve vertical variation in the canopy density, and large enough in the horizontal plane to include several stems ( $> \Delta S$ ).

Using the double-averaging method, the streamwise momentum equation becomes

$$\frac{D \langle \bar{u} \rangle}{Dt} = g \sin \theta - \frac{1}{\rho} \frac{\partial \langle \bar{p} \rangle}{\partial x} - \underbrace{\frac{\partial}{\partial z} \langle \bar{u}' w' \rangle}_{\text{(i)}} - \underbrace{\frac{\partial}{\partial z} \langle \bar{u}'' \bar{w}'' \rangle}_{\text{(ii)}} + \underbrace{\nu \frac{\partial^2 \langle \bar{u} \rangle}{\partial z^2}}_{\text{(iii)}} - D_x. \quad (2)$$

Here  $\rho$  is the water density,  $\nu$  is the kinematic viscosity,  $\theta$  is the bed slope, and  $g$  is the gravitational acceleration. Term i is the spatial average of the Reynolds stress. Term ii, called the dispersive stress, is the momentum flux associated with spatial correlations in the time-averaged velocity field. Poggi et al. (2004a) have shown that the dispersive stress is less than 10% of the Reynolds stress (term i) for  $\lambda_f = ab > 0.1$ . Term iii is the viscous stress associated with the spatial variation in  $\langle \bar{u} \rangle$ . The final term,  $D_x$ , is the spatially averaged drag associated with the canopy elements, which is often represented by a quadratic drag law (e.g., Kaimal & Finnigan 1994, p. 95):

$$D_x = \frac{1}{2} \frac{C_D a}{1 - \phi} \langle \bar{u} \rangle |\langle \bar{u} \rangle|, \quad (3)$$

where  $C_D$  is the canopy drag coefficient. Because the drag acts on the fluid within the canopy, which occupies only  $(1 - \phi)$  of the total volume, the drag is divided by the factor  $(1 - \phi)$ . The canopy drag length scale,  $L_c$ , is defined from the quadratic drag law, i.e., based on dimensional reasoning  $D_x = \langle \bar{u} \rangle^2 / L_c$  (Belcher et al. 2003). From Equation 3,

$$L_c = \frac{2(1 - \phi)}{C_D a}. \quad (4)$$

This represents the length scale over which the mean and turbulent flow components adjust to canopy drag. Because most aquatic canopies have high porosity ( $\phi < 0.1$ ), this scale is commonly approximated by  $(C_D a)^{-1}$ .

The drag coefficient,  $C_D$ , is affected by the canopy density,  $a$ ; the element Reynolds number,  $Re_d = \langle \bar{u} \rangle d / \nu$ ; and the morphology of the individual canopy elements. A review of  $C_D$ 's dependency on the Reynolds number and the canopy density can be found in Tanino & Nepf (2008a) and Nepf (2012). A linear drag law provides a better fit for rigid vegetation under low-element Reynolds number [ $Re_d < 50$  (Tanino et al. 2005)]. The Darcy-Forchheimer equation (e.g., Whitaker 1996) has also been used to describe drag in wetlands (Oldham & Sturman 2001) and coral canopies (Lowe et al. 2008). For flexible vegetation, the posture of the blade is affected

### Submerged

**vegetation:** rooted vegetation with a vertical extent less than the water depth

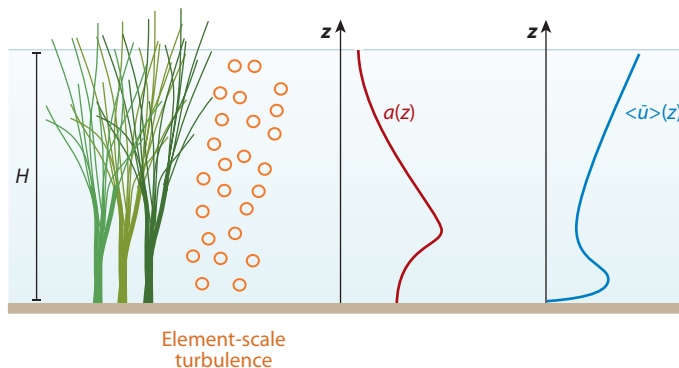


**Figure 1**

Emergent canopy of marsh grass, with vertical ( $z$ ) profiles of leaf area index,  $a$ , and longitudinal velocity,  $\langle \bar{u} \rangle$ . The velocity profile varies inversely with  $a$ , creating a velocity maximum close to the bed, below the level at which branching begins.

by the flow speed, a phenomenon called reconfiguration. As velocity increases, the blades are pushed over into more streamlined positions so that the drag force increases more slowly with increasing velocity than predicted by the quadratic drag law. The impact of a changing plant shape on the drag force has been represented by altering the exponent in the drag law, while holding  $a$ , the frontal area, constant at the undisturbed (no flow) value,  $a_0$ . Specifically, the square power in Equation 3 is replaced with a variable power  $2 + E$ . The exponent  $E$  assumes values between zero (rigid blade) and  $-2$  (extremely flexible), depending on the type of vegetation (see, e.g., Vogel 1994, chapter 6; Alben et al. 2002; Green 2005; O'Hare et al. 2007; Sand-Jensen 2008; Gosselin et al. 2010). In practice, it is difficult to characterize the frontal area  $a$  for real plants, which has led to contradictory results in the dependency of drag on velocity [e.g., see discussion of Sand-Jensen (2003) by Sukhodolov (2005), Green (2005), and Statzner et al. (2006)].

## EMERGENT CANOPIES

An emergent canopy fills the entire water depth,  $H$ , and typically penetrates the water surface. This type of canopy occurs in tidal marshes, kelp forests, and seagrass meadows during periods of low tide. Emergent canopies impose structure on both the mean and turbulent flow over the entire water column. The canopy dissipates eddies with scales greater than the stem scales of  $\Delta S$  and  $d$ , while contributing additional turbulent energy at these stem scales (**Figure 1**). As a result, the dominant turbulent length scale within a canopy is shifted downward from analogous conditions without vegetation. In an open channel (no vegetation), eddies scale with the water depth,  $H$ . In a channel with rigid vegetation, the integral length scale of the turbulence,  $\ell$ , is set by the smaller of the stem diameter,  $d$ , or the average distance to the nearest neighboring stem,  $S_n$ , regardless of the water depth (Tanino & Nepf 2008b). In a square array of stems, the average spacing and the average nearest-neighbor spacing are the same,  $\Delta S = S_n$ , but in a random array,  $S_n < \Delta S$ . For  $d \leq S_n$ , turbulence is generated within stem wakes (if the Reynolds number is sufficient) so that  $\ell = d$ . For  $d > S_n$ , turbulence is generated within the pore channels so that  $\ell = S_n$ . These two regimes are depicted in **Figure 2a**. Even for solid volume fractions as low as 0.6% ( $a = 0.01 \text{ cm}^{-1}$ ), the production of turbulence by the canopy exceeds the production by the bed shear over most of the flow depth (Nepf et al. 1997, Burke & Stolzenbach 1983, Lopez & Garcia 1998).

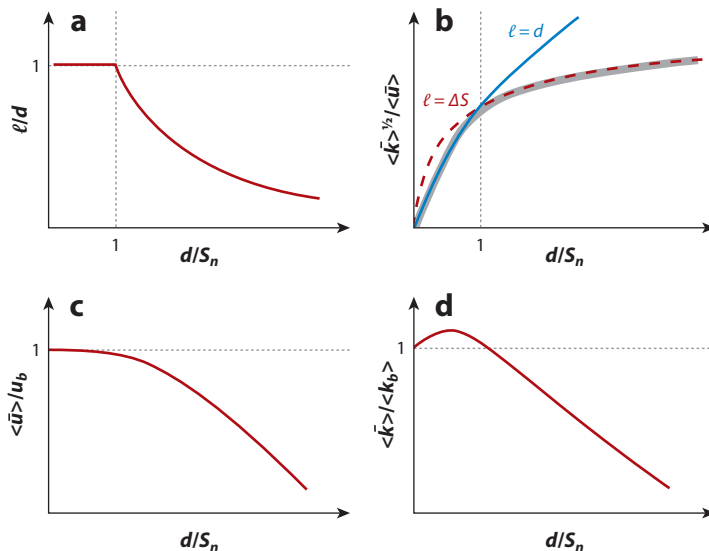


**Figure 2**

Changes in flow properties with increasing stem density. (a) The integral scale of turbulence,  $\ell$ , is set by the smaller of two canopy scales: the stem diameter,  $d$ , and the nearest-neighbor stem spacing,  $S_n$ . If  $d \leq S_n$ ,  $\ell = d$ . If  $d \geq S_n$ ,  $\ell = S_n$ . (b) The turbulence intensity, given by Equation 7, depends on the integral length scale of the turbulence. If  $d < S_n$ , the turbulence intensity increases rapidly with increasing stem density because  $a\ell \approx d^2/S_n^2$ . If  $d > S_n$ , the turbulence intensity increases more slowly, as  $a\ell \approx d/S_n$ . Changes in (c) velocity and (d) turbulent kinetic energy, with increasing stem density, are shown relative to values for a bare bed (subscript  $b$ ) with the same forcing. Based on figure 10 in Nepf (2012), reproduced with the kind permission of Elsevier Press.

Therefore, the turbulence level cannot be predicted from the bed-friction velocity, as it can for open-channel flow. Instead, it is a function of the canopy drag, as described below.

Vortex generation by stem wakes and/or in pore channels drains energy from the mean flow (expressed in terms of canopy drag) and feeds it into the turbulent kinetic energy. If this conversion is 100% efficient, then the rate at which turbulent energy is produced,  $P_w$ , is equal to the rate at which mean flow energy is extracted, i.e., the rate of work done by the flow against canopy drag (e.g., Raupach & Shaw 1982):

$$P_w = \frac{1}{2} C_D a \langle \bar{u} \rangle^3. \quad (5)$$

In fact, only the form drag is converted into turbulent kinetic energy. The viscous drag component is immediately dissipated to heat. For stiff canopies, i.e., most emergent canopies, and  $Re_d > \approx 200$ , the majority of the drag is form drag, and Equation 5 is a reasonable approximation (Tanino & Nepf 2008a,b). In contrast, Nikora & Nikora (2007) suggested that for flexible canopies, which are typically submerged, the drag is predominantly viscous, and Equation 5 would be an overestimate of stem-scale turbulence production. The relative contributions of viscous drag and form drag depend on the morphology and alignment (streamlined versus bluff) of the blades and stems within the canopy.

Within a homogenous emergent canopy, transport terms are negligible, and the wake production in Equation 5 is balanced by viscous dissipation,  $\varepsilon$ , i.e.,  $P_w = \varepsilon$ . In addition, for turbulent kinetic energy,  $k$ , the dissipation rate within the canopy has the scale (Tennekes & Lumley 1972)

$$\varepsilon \sim \langle \bar{k} \rangle^{3/2} \ell^{-1}. \quad (6)$$

#### Stem-scale turbulence:

turbulence generated in the wakes of individual stems and branches

Connecting Equations 5 and 6, the turbulence intensity in the canopy is

$$\frac{\sqrt{\langle k \rangle}}{\langle \bar{u} \rangle} \sim (C_D a \ell)^{1/3}. \quad (7)$$

As described above, the turbulence length scale,  $\ell$ , is set by the smaller of the stem diameter,  $d$ , and the nearest-neighbor stem spacing,  $S_n$ . In a canopy of low solid volume fraction, or specifically  $S_n > d$ , the turbulence intensity increases rapidly with increasing canopy density (**Figure 2b**) because  $\ell = d$ , and thus  $a\ell \approx d^2/S_n^2$  in Equation 7. In a canopy of high solid volume fraction,  $S_n < d$ , the turbulence intensity increases more slowly because  $\ell = S_n$ , and thus  $a\ell \approx d/S_n$  in Equation 7.

Within an emergent canopy, the momentum equation (Equation 2) will generally simplify to a balance between potential forcing (associated with hydrostatic pressure or bed slope) and canopy drag. First, viscous stress,  $\nu \partial^2 \langle \bar{u} \rangle / \partial z^2$ , is negligible compared to vegetative drag over most of the depth, excluding a thin layer near the bed of a scale comparable to the stem diameter,  $d$  (Nepf & Koch 1999). Second, as discussed above, the eddy length scale is small compared to the water depth, which limits the turbulence flux of momentum; i.e., the turbulence stresses are typically negligible. For example, from numerical experiments, the eddy scales are 1%–3% of the water depth, and turbulent stresses are only 2% of the total drag for  $aH = 0.1$  (Burke & Stolzenbach 1983). Similar ratios have been measured in model emergent canopies (Nepf & Vivoni 2000). A notable exception occurs near the surface, as wind-generated stress can sometimes play a role in the momentum balance (Jenter & Duff 1999). Third, we assume that dispersive fluxes are negligible because the canopy density is commonly above the threshold  $ab > 0.1$  suggested by Poggi et al. (2004a). For steady, uniform flow, the momentum equation then reduces to

$$g \left( \frac{\partial H}{\partial x} + \sin \theta \right) = -\frac{1}{2} \frac{C_D a}{1 - \phi} \langle \bar{u} \rangle |\langle \bar{u} \rangle| = -\frac{\langle \bar{u} \rangle |\langle \bar{u} \rangle|}{L_c}. \quad (8)$$

The hydrostatic pressure and potential gradients that drive the flow (left-hand side of Equation 8) are not functions of the vertical coordinate,  $z$ . The right-hand side then must also be independent of  $z$  so that the velocity varies inversely with the frontal area,  $a$ , and in proportion to the canopy-drag length scale,  $L_c$ . For plants with a distinct basal stem, this produces a velocity maximum close to the bed because  $a$  is reduced below the level at which branching begins (**Figure 1**). A near-bed velocity maximum is often observed in the marsh grass *Spartina alterniflora* (Leonard & Luther 1995, Leonard & Croft 2006). In contrast, the more vine-like *Atriplex portulacoides* has leaves (and thus  $C_D a$ ) that are more evenly distributed over depth, and the resulting velocity profile is uniform over depth (Leonard & Reed 2002).

Equation 8 implies that the velocity profile within an emergent canopy has a self-similar form. When the velocity is normalized by its value at an arbitrary reference depth, denoted by the subscript *ref*, the normalized profiles collapse together, regardless of the absolute magnitude of the current. The shape of the normalized profile depends on the vertical distribution of  $L_c$ :

$$\frac{\langle \bar{u} \rangle}{\langle \bar{u} \rangle_{ref}} = \sqrt{\frac{L_c}{L_{c-ref}}} \approx \sqrt{\frac{(C_D a)_{ref}}{(C_D a)}}, \quad (9)$$

where the right-most approximation holds in most salt- and freshwater wetlands canopies, for which the canopy solid volume fraction is small ( $\phi < 0.1$ ) so that  $(1 - \phi) \approx 1$ . A self-similar velocity structure was confirmed by measurements in a coastal marsh (Lightbody & Nepf 2006) and in the freshwater wetlands of the Everglades (Huang et al. 2008). The normalization in Equation 9 provides an important tool for extrapolating a full velocity profile from records at a single vertical position.

An interesting nonlinear behavior emerges when we compare flow conditions under different canopy densities but with the same potential and/or pressure gradient. To include the no-canopy limit (i.e., bare bed), one must incorporate the bed resistance into the momentum balance. **Figure 2c,d** depicts the change in velocity and turbulent kinetic energy, respectively, relative to bare-bed conditions, with the latter denoted by the subscript  $b$ . The details of this comparison have been given by Nepf (1999). Because the vegetation offers additional resistance, the velocity within the canopy is always less than that over a bare bed, and the velocity ratio,  $\langle \bar{u} \rangle / u_b$ , decreases as the vegetation density increases (**Figure 2c**). Changes in turbulent kinetic energy with increasing vegetation density reflect the competing effects of the reduced velocity and the additional turbulence production in stem wakes (Equation 7). These opposing tendencies produce a nonlinear response in which the turbulence levels initially increase with increasing canopy density but decrease as  $a$  increases further (**Figure 2d**). This nonlinear response was predicted numerically for flow through emergent vegetation (Burke & Stolzenbach 1983) and within submerged roughness elements (Eckman 1990). It has been observed in flume studies of flow through real stems of *Zostera marina* (Gambi et al. 1990). The enhanced turbulence levels in sparse canopies have important implications for canopy ecology. An increase in turbulence, particularly element-scale turbulence, could benefit vegetation by augmenting nutrient uptake and/or gas exchange (Anderson & Charters 1982) and similarly enhance uptake by microbes living on plant surfaces (e.g., Gantzer et al. 1991). Significant contributions to the turbulence intensity from stem-scale turbulence have also been observed in beds of channel macrophytes (Naden et al. 2006).

It is commonly expected that dense patches of vegetation, because they damp flow and turbulence, are associated with muddification, an increase in fine particles and organic content of the underlying sediment relative to adjacent bare-bed conditions. Recently, van Katwijk et al. (2010) observed that sparse patches of vegetation are associated with sandification, a decrease in fine particles and organic matter, and they attribute this to higher levels of turbulence within the sparse patch, relative to adjacent bare regions. A transition from a tendency for sandification (elevated turbulence) to a tendency for muddification (diminished turbulence intensity) with increasing canopy density is consistent with the nonlinear model shown in **Figure 2d**.

## SUBMERGED CANOPIES

The velocity within a submerged canopy has a range of behavior depending on the relative depth of submergence, defined as the ratio of flow depth,  $H$ , to canopy height,  $b$ . The flow within the canopy is driven by the turbulent stress at the top of the canopy as well as by the gradients of pressure and gravitational potential (bed slope). The relative importance of these driving forces varies with the depth of submergence (Nepf & Vivoni 2000):

$$\frac{\text{turbulent stress}}{\text{pressure gradient}} \sim \frac{H}{b} - 1. \quad (10)$$

Three classes of canopy flow can be defined from Equation 10: deeply submerged or unconfined ( $H/b > 10$ ), shallow submergence ( $H/b < 5$ ), and emergent ( $H/b = 1$ ). A great deal is known about unconfined canopy flow based on work in terrestrial canopies (e.g., Raupach et al. 1996, Finnigan 2000, Belcher et al. 2012). When unconfined, the flow within a canopy is driven by the turbulent stress at the top of the canopy, i.e., by the vertical turbulent transport of momentum from the overflow, with negligible contribution from pressure gradients. The terrestrial canopy model can be applied to aquatic canopies that are deeply submerged. However, because of the limitation of light penetration, most submerged aquatic canopies occur in the range of shallow submergence

---

**Emergent vegetation:** rooted vegetation that penetrates the free surface and thus occupies the full water depth

---



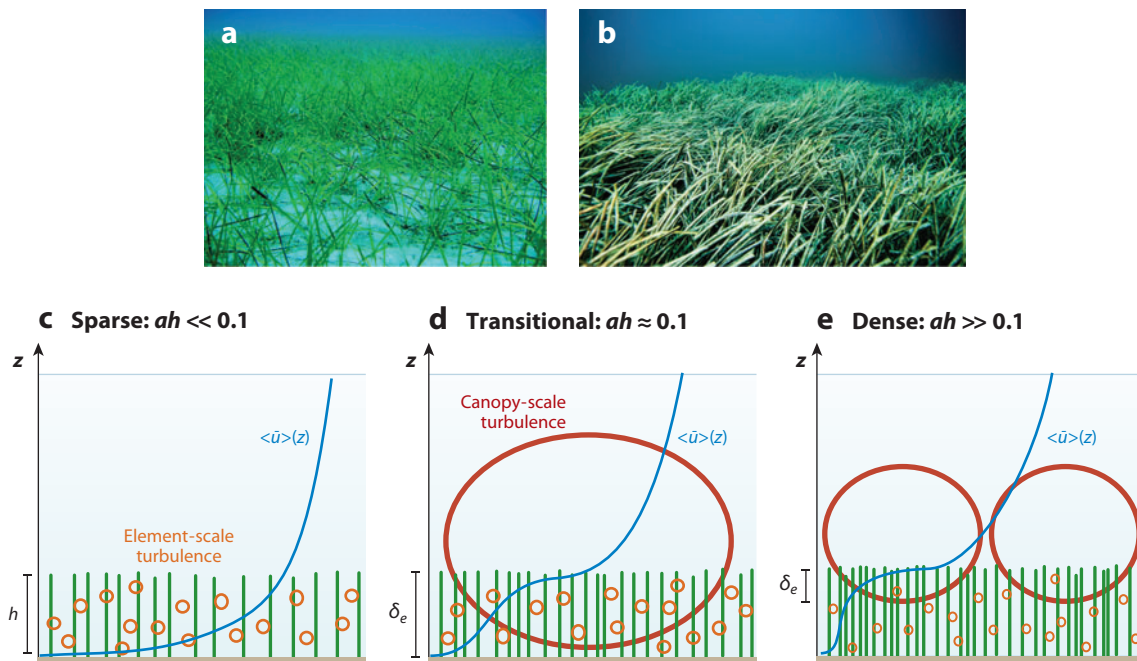


**Figure 3**

(a) The seagrass *Cymodocea nodosa* at low stem density. (b) The seagrass *Posidonia oceanica* at high stem density. Photos by Eduardo Infantes Oanes. Vertical ( $z$ ) profiles of longitudinal velocity and dominant turbulence scales are shown for (c) a sparse canopy ( $ah \ll 0.1$ ), (d) a transitional canopy ( $ah \approx 0.1$ ), and (e) a dense canopy ( $ah \gg 0.1$ ), where  $h$  is the submerged canopy height. For  $ah \geq 0.1$ , a region of strong shear at the top of the canopy generates canopy-scale turbulence. Element-scale (stem-scale) turbulence is generated within the canopy.

$H/b < 5$  (e.g., Chambers & Kalff 1985, Duarte 1991), for which both turbulent stress and potential gradients are important in driving flow in the canopy. For emergent conditions ( $H/b = 1$ ), flow is driven by the potential gradients, as described in the previous section.

For a submerged canopy, there are two limits of behavior, depending on the relative importance of the bed drag and the canopy drag. If the canopy drag is small compared with the bed drag, then the velocity follows a turbulent boundary-layer profile, with the vegetation contributing to the bed roughness (sparse canopy; **Figure 3c**). If the canopy drag is large compared to the bed drag, the discontinuity in drag that occurs at the top of the canopy ( $z = b$ ) generates a region of shear resembling a free shear layer with an inflection point near the top of the canopy (dense canopy; **Figure 3d,e**). From scaling arguments, Belcher et al. (2003) predicted that the transition between the sparse and dense regimes occurs at the roughness density  $\lambda_f = ah = 0.1$ . Numerical simulations by Coceal & Belcher (2004, figure 4) suggest that the transition occurs at  $L_c/b = 5$ , which corresponds to  $\lambda_f = 0.15$ , for their parameter set ( $C_D = 2$ ,  $\phi = 0.25$ ). On the basis of measured velocity profiles in aquatic systems (Nepf et al. 2007, and references therein), the profile exhibits a boundary-layer form with no inflection point if  $C_D ah < 0.04$ . A pronounced inflection point appears at the top of the canopy for  $C_D ah > 0.1$ . Because  $C_D \approx 1$  in most of the studies considered, these limits are consistent with the scaling and numerical estimates given above. Note that this review considers only unidirectional flow. In flow conditions dominated by waves, the canopy drag may have little impact on the wave-induced velocity (see the sidebar, Waves over Submerged Canopies).



## WAVES OVER SUBMERGED CANOPIES

Because the flow beneath waves is unsteady, inertial forces can be comparable to or larger than the canopy drag at high wave frequencies, including typical wind-wave frequencies. For these conditions, the wave velocity is not significantly damped within the canopy, in contrast to the large degree of damping observed for dense canopies in a unidirectional flow (**Figure 3**). Furthermore, in analogy to viscous boundary streaming, canopy drag induces a nonzero wave stress, which in turn generates a mean mass drift within the canopy. Steady currents with magnitudes up to 40% of the near-bed orbital velocity have been measured in model canopies (Lowe et al. 2005, Luhar et al. 2010).

In this article, we focus on the dense canopy condition ( $ab > 0.1$ ). For these canopies, Raupach et al. (1996) demonstrated a similarity between canopy shear layers and free shear layers. In a free shear layer, the velocity profile contains an inflection point, which triggers a flow instability that in turn leads to the generation of Kelvin-Helmholtz vortices (e.g., Brown & Roshko 1974, Winant & Browand 1974). These structures dominate the transfer of momentum between the high-speed and low-speed streams, and their size sets the length scale of the shear layer. For dense submerged canopies ( $ab \geq 0.1$ ), the momentum absorption by the canopy is sufficient to produce an inflection point in the velocity profile, which, as in free shear layers, leads to the generation of Kelvin-Helmholtz vortices (**Figure 3d,e**). These vortices are called canopy-scale turbulence to distinguish it from the much-larger boundary-layer turbulence, which may form above a deeply submerged or unconfined canopy, and the much smaller stem-scale turbulence.

Over a deeply submerged (or terrestrial) canopy ( $H/b > 10$ ), the canopy-scale vortices are highly three dimensional owing to their interaction with the larger boundary-layer turbulence, which stretches the canopy-scale vortices, enhancing secondary instabilities (Fitzmaurice et al. 2004, Finnigan et al. 2009). However, with shallow submergence ( $H/b \leq 5$ ), which is common in aquatic systems, larger-scale boundary-layer turbulence is not present, and the canopy-scale vortices dominate the turbulence field, both within and above the canopy (Ghisalberti & Nepf 2005, 2009). For shallow submergence, the canopy-scale turbulence is also more coherent (less than three dimensional) than that observed with deeply submerged (or terrestrial) conditions. However, in both cases, the canopy-scale vortices dominate the vertical transport at the canopy interface (e.g., Gao et al. 1989, Finnigan 2000, Ghisalberti & Nepf 2002).

In a free shear layer, the vortices grow continually downstream, predominantly through vortex pairing (Winant & Browand 1974). In canopy shear layers, however, the vortices reach a fixed scale and a fixed penetration into the canopy ( $\delta_e$  in **Figure 3d,e**) at a short distance from the canopy's leading edge (Ghisalberti & Nepf 2004). On the basis of measurements with a flexible model of the seagrass *Z. marina* ( $a = 5.7 \text{ m}^{-1}$ ), a fixed shear-layer scale is reached at a distance of  $10b$  from the leading edge of the meadow (Ghisalberti 2000). The fixed vortex and shear-layer scale is reached when the shear production that feeds energy into the canopy-scale vortices is balanced by dissipation by canopy drag. This energy balance predicts the following length scale, which has been verified by laboratory observations (Nepf et al. 2007):

$$\delta_e = \frac{0.23 \pm 0.6}{C_D a}. \quad (11)$$

Let us recall that  $C_D ab \geq 0.1$  is required to produce shear-layer vortices, so Equation 11 applies only to those canopies. In the range  $C_D ab = 0.1$  to  $0.23$ , the shear-layer vortices penetrate to the

---

**Canopy shear layer:** the region of velocity shear generated by the drag discontinuity at top of the submerged canopy

**Canopy-scale turbulence:** vortices generated within the canopy shear layer by Kelvin-Helmholtz instability

---

bed,  $\delta_e = b$ , creating a highly turbulent condition over the entire canopy height (**Figure 3d**). At higher values of  $C_{Dab}$ , the canopy-scale vortices do not penetrate to the bed,  $\delta_e < b$  (**Figure 3e**).

The scaling  $\delta_e \sim a^{-1}$  has been observed in flows near porous layers over a wide range of physical scales, from granular beds to terrestrial forests and urban canopies (Ghisalberti 2009). However, the scale relation must break down when  $(C_{Da})^{-1}$  approaches the scale of the canopy elements,  $d$ , because  $a$  is defined only as an average over multiple elements. For rigid cylinders, when  $(C_{Da})^{-1}$  is less than  $2d$ , the penetration scale transitions to a constant  $\delta_e \approx 2d$  (White & Nepf 2007). The depth of submergence,  $H/b$ , can also affect the penetration length scale. For  $H/b < 2$ ,  $\delta_e$  is diminished from Equation 11, as interaction with the water surface diminishes the strength and scale of the vortices (Nepf & Vivoni 2000, Okamoto & Nezu 2009).

The penetration length,  $\delta_e$ , segregates the canopy into an upper layer of strong turbulence and rapid renewal and a lower layer of weak turbulence and slow renewal (Nepf & Vivoni 2000). Flushing of the upper canopy is enhanced by the canopy-scale vortices that penetrate this region (**Figure 3e**). In contrast, turbulence in the lower canopy ( $z < b - \delta_e$ ) is generated in stem wakes and has a significantly smaller scale, set by the stem diameters and spacing. Canopies for which  $\delta_e/b < 1$  (**Figure 3e**) shield the bed from strong turbulence and turbulent stress. Because turbulence near the bed plays a role in resuspension, these dense canopies are expected to reduce resuspension and trap sediment. Consistent with this, Moore (2004) observed that resuspension within a seagrass meadow was reduced, relative to bare-bed conditions, only when the above-ground biomass per unit area was greater than  $100 \text{ g m}^{-2}$  (dry mass). This biomass corresponds to  $ab = 0.4$  (Luhar et al. 2008). Using  $C_D \approx 1$ , one sees that this canopy density is consistent with the transition implied by Equation 11. We note that the transition in near-bed turbulence and resuspension does not occur abruptly at  $C_{Dab} = 0.23$  but occurs gradually with increasing  $C_{Dab}$  above this value, as the canopy-scale vortices are progressively pushed further from the bed. Because of the reduced near-bed turbulence, dense canopies can promote sediment retention. In sandy regions, which tend to be nutrient poor, the preferential retention of fines and organic material (i.e., muddification) enhances the supply of nutrients to the canopy so that dense canopies provide a positive feedback to canopy health in sandy regions. In contrast, in regions with muddy substrate, which is more susceptible to anoxia, sparse meadows ( $C_{Dab} \leq 0.23$ ) may be more successful because the enhanced near-bed turbulence removes fines, leading to a sandier substrate that is less prone to anoxia.

## Flexible Canopies and Monami

Under some conditions, the canopy-scale vortices produce sufficient instantaneous drag to overcome the buoyancy and rigidity of individual blades. The passage of the traveling vortices then causes a local depression in the canopy, which travels along the canopy interface, in sync with the traveling vortices (**Figure 4a**). This progressive waving of canopy blades is called a monami (Ackerman & Okubo 1993). It has been observed to occur extensively in the field (e.g., Fonseca & Kenworthy 1987, Ackerman & Okubo 1993, Grizzle et al. 1996). The frequency of the monami matches the frequency of vortex passage, which is given by instability theory (Ikeda & Kanazawa 1996, Ghisalberti & Nepf 2002). However, if the instantaneous drag associated with the canopy-scale vortices is not sufficient to depress individual blades, the monami does not occur, even though the canopy-scale vortices are present.

To understand the connection between the canopy-shear-layer vortices and the monami, it is useful to consider the differences between the free shear layer and the canopy shear layer. Free-shear-layer vortices are symmetric around the inflection point ( $z_i$ ), and their translation speed,  $U_v$ , matches the velocity at the inflection point,  $U_i$ . Because these vortices rotate faster than they translate, the lower region of the layer experiences a negative velocity perturbation as a

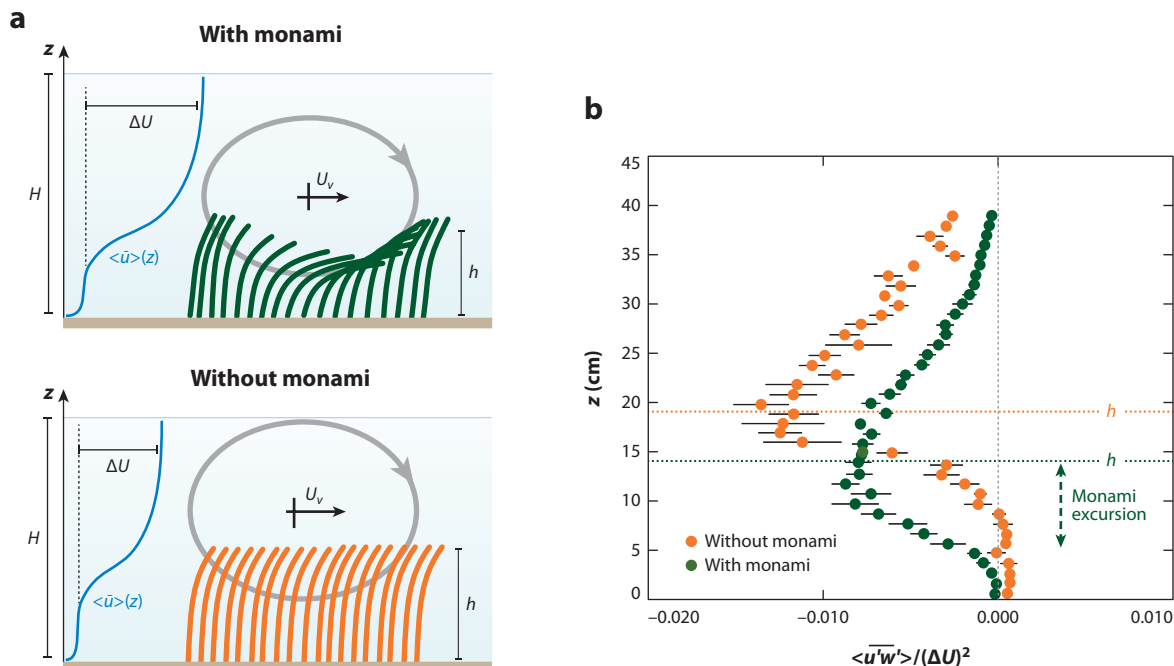


**Figure 4**

(a) For dense submerged canopies ( $ah > 0.1$ ), the drag discontinuity at the top of the canopy generates a region of shear resembling a free shear layer, which in turn generates canopy-scale vortices by Kelvin-Helmholtz instability. The passage of these canopy-scale vortices over the canopy may generate a progressive waving of the canopy that is called a monami (*green canopy*). If the shear-layer vortices are too weak, the canopy will bend but not wave (*orange canopy*). (b) Profiles of normalized turbulent stress in and above a flexible canopy for two flow conditions, based on data from Ghisalberti & Nepf (2006). With the weaker current, no monami occurs (*orange dots*). With a stronger current, a monami is produced (*green dots*). The vertical excursion of the canopy interface associated with the monami is shown with the dashed double-arrow. Under the stronger current (*green dots*), the individual blades are deflected further, reducing the mean canopy height ( $h$ ), relative to the condition with the weaker current (*orange dots*).

vortex passes (e.g., Dimotakis et al. 1981, Ho et al. 1991). In a canopy shear layer, the inflection point corresponds to the top of the canopy ( $z_i \approx h$ ) so that the velocity at the inflection point is  $U_i = U_b = \langle \bar{u} \rangle_b$ . However, because of the canopy drag, the vortices are displaced upward, relative to the inflection point. As a result, the translation speed of the vortex is higher than the velocity at the inflection point, i.e.,  $U_v \geq U_i = U_b$  (Ikeda & Kanazawa 1996). The velocity ratio  $U_v/U_b$  increases with increasing depth of submergence ( $H/h$ ), up to  $U_v/U_b = 1.8$  observed at  $H/h = 4.5$  (Ghisalberti & Nepf 2002). In terrestrial canopies,  $U_v/U_b$  is also 1.8 (Finnigan 1979), suggesting that this is the asymptotic value for unconfined canopies. Furthermore, the canopy drag causes the vortices to rotate more slowly than vortices formed in a free shear layer of comparable shear strength. The translation speed of the vortex is sufficiently large compared to its rotation so that as the front of the vortex passes, a strong sweep ( $u > 0$ ,  $w < 0$ ) invades the canopy (Ghisalberti & Nepf 2002). The monami is generated as the sweep deflects the canopy forward and downward. The connection between the velocity field and the plant motion has been described by Ghisalberti & Nepf (2006) and Okamoto & Nezu (2009).

The flexibility of the canopy and the presence of monami affect the turbulent exchange between the canopy and the overflow. This can be seen in the profiles of Reynolds stress, normalized by the square of the velocity difference ( $\Delta U$ ) between the canopy and overflow, which is a measure

of momentum exchange efficiency. The two profiles shown in **Figure 4b** are measured with the same flexible canopy [ $a \approx 0.052 \text{ cm}^{-1}$ , and  $ab = 1$  when erect, described by Ghisalberti & Nepf (2005)]. The vertical axis is dimensional to emphasize the vertical shift associated with the greater deflection of the canopy under the higher flow condition. In the weaker-flow case ( $U_b = 1.7 \text{ cm s}^{-1}$ ), canopy-scale vortices are produced but are too weak to deflect the blades, and no monami occurs. In the stronger-flow case ( $U_b = 7.9 \text{ cm s}^{-1}$ ), the canopy deflection is larger (smaller  $b$ ), and the canopy-scale vortices are strong enough to trigger a monami. The monami excursion amplitude is noted in the figure. The combination of deflection and monami allows the turbulent flux to penetrate closer to the bed, which leads to greater in-canopy flow speed (see also Ghisalberti & Nepf 2009).

Whereas a monami allows for a deeper penetration of stress, the momentum transfer is less efficient. For example, the maximum normalized stress is  $\langle \overline{u'w'} \rangle / (\Delta U)^2 = 0.013$  for the stationary canopy but is only 0.008 with a monami present (**Figure 4b**). A rigid canopy produces even more efficient exchange, with a peak normalized stress of 0.017 (Ghisalberti & Nepf 2005). The diminished exchange efficiency occurs because the vortices are smaller and weaker in the presence of a monami and also weaker above a flexible canopy compared with a rigid canopy of similar geometry (see detailed discussion in Ghisalberti & Nepf 2006).

## Mean Velocity Profile

Sufficiently far above a submerged canopy ( $z > 2b$ ), the velocity profile is logarithmic (see Kaimal & Finnigan 1994, and reference therein):

$$\langle \bar{u} \rangle = \frac{u_*}{\kappa} \ln \left( \frac{z - z_m}{z_o} \right), \quad (12)$$

with  $\kappa = 0.4$  (von Kármán constant). The horizontal average (in angled brackets) is not strictly needed above the canopy but is retained for consistency with the equations within the canopy. The friction velocity,  $u_*$ , is related to the Reynolds stress at the top of the canopy,  $u_*^2 = \langle \overline{u'w'} \rangle_b$ . The parameters  $z_m$  and  $z_o$  are the displacement and roughness heights, respectively, both of which depend on the canopy roughness density,  $ab$ . On the basis of studies with both model and real vegetation, a simple estimate for friction velocity is  $u_* = [gS(H - b)]^{0.5}$ , with  $S = \partial H / \partial x + \sin \theta$  (Murphy et al. 2007). If the vegetation is flexible, then  $b$  is the mean deflected height of the canopy (Jarvela 2005). However, if the depth of submergence is small, compared to the displacement height, the following estimator is more accurate:  $u_* = [gS(H - z_m)]^{0.5}$  (Nepf & Vivoni 2000).

Let us recall that the penetration length scale,  $\delta_e$ , describes the distance over which turbulent stress penetrates the canopy from above. Similarly, the displacement height is the centroid of momentum penetration into the canopy (Thom 1971). This similarity suggests the physically intuitive scaling

$$\frac{z_m}{b} \approx 1 - \frac{1}{2} \frac{\delta_e}{b} = 1 - \frac{0.1}{C_D ab}, \quad (13)$$

which has been confirmed for  $ab \approx 0.2$  to 3 (Luhar et al. 2008). For  $ab > 1$ , the displacement thickness tends toward  $z_m \approx b$ , indicating that essentially the entire canopy is cut off from the overflow. In addition,  $z_m$  goes to zero at  $ab = 0.1$ . When  $z_m = 0$ , the velocity profile has no inflection point (**Figure 3c**), consistent with the observation that  $ab > 0.1$  is required to produce an inflection point in measured velocity profiles (**Figure 3d,e**).

The dependency of the roughness height,  $z_o$ , on the canopy density,  $ab$ , differs significantly above and below the threshold of  $ab = 0.1$  (e.g., Raupach et al. 1980, MacDonald et al. 1998,

Jimenez 2004, Luhar et al. 2008). In the sparse-canopy range ( $ab < 0.1$ ), the roughness height increases with increasing  $ab$ . In sparse canopies, the flow penetrates the full canopy so that  $z_o$  is proportional to the drag imparted by the full canopy,  $C_D ab$ , i.e.,  $z_o/b \sim C_D ab$ . In contrast, for dense canopies ( $ab > 0.1$ ), the roughness height decreases with increasing  $ab$ . The effective height of the canopy, as seen by the overflow, is the penetration scale,  $\delta_e$ . The roughness height depends on this effective height, rather than the canopy height, so that  $z_o \sim \delta_e \sim a^{-1}$ . For example, data summarized by Luhar et al. (2008) suggest that for  $ab > 0.1$ ,  $z_o = (0.04 \pm 0.02)a^{-1}$ .

The logarithmic profile form is based on equilibrium turbulence such that dissipation and production are locally in balance (e.g., Tennekes & Lumley 1972). Largely because of the vertical transport provided by the shear-layer structures, this condition is not met for some distance above the canopy, called the roughness sublayer. For very shallow submergence,  $H/b \leq 1.5$ , the roughness sublayer extends to the surface, and a logarithmic structure is not observed above the canopy.

The flow within a submerged canopy is driven by a combination of the turbulent, dispersive, and viscous (usually negligible) stresses generated by the overflow, as well as the potential gradient associated with the hydrostatic pressure gradient and the bed slope. Below the penetration of turbulent and dispersive stress ( $z < b - \delta_e$ ), conservation of linear momentum reduces to a balance between potential gradients and the sum of the canopy and the bed drag. Assuming that the canopy drag is much larger than the bed drag, this balance yields the following mean velocity:

$$\langle \bar{u} \rangle = U_1 = \sqrt{\frac{2g(\partial H / \partial x + \sin \theta)}{C_D a}}. \quad (14)$$

This is the same momentum balance observed for emergent canopies. So, again, if the canopy density  $a$  or drag coefficient  $C_D$  is a function of  $z$ , the velocity will vary inversely; i.e., the velocity will be highest where  $C_D a$  is lowest.

In the upper canopy ( $b - \delta_e < z < b$ ), flow is driven by both potential gradients and turbulent stress. The stress-driven component is derived by simplifying the momentum equation (Equation 2) to a balance of the canopy drag and turbulent stress and modeling the turbulent stress with a mixing length model,  $\langle \overline{u'w'} \rangle = \ell_m^2 (\partial \langle \bar{u} \rangle / \partial z)^2$  (e.g., Inoue 1963, Cionco 1965). This yields the exponential velocity profile observed in terrestrial canopies. In aquatic canopies, the potential-driven component is also important in the upper canopy. Combining the stress-driven and potential-driven components, the upper canopy velocity profile is

$$\langle \bar{u} \rangle = U_1 + (U_b - U_1) \exp[-K_u(b - z)], \quad (15)$$

with  $U_b = \langle \bar{u} \rangle$  at the top of the canopy, and constant  $K_u = \beta / \ell_m$ , with  $\beta = u^*/U_b$ . It is physically intuitive that the mixing length should be related to the penetration of shear-layer vortices into the canopy, i.e.,  $\ell_m \sim \delta_e \sim (C_D a)^{-1}$ . Harman & Finnigan (2007) suggest  $\ell_m = 2\beta^3(C_D a)^{-1}$ , or  $K_u = C_D a / (2\beta^2)$ . For rigid canopies in water,  $\beta = 0.24 \pm 0.02$  (standard error; data in Ghisalberti & Nepf 2005), which predicts  $K_u = (8.7 \pm 1.4)C_D a$ . This predicted value agrees with the observed decay scale constant,  $K_u = (9 \pm 2)C_D a$ , extracted from measured velocity profiles in Ghisalberti (2005). In the dense canopy limit,  $\beta$  has no dependency on the canopy density (Ghisalberti & Nepf 2005), but it declines as the transition to the sparse canopy limit ( $ab < 0.1$ ) is approached, i.e., as the canopy-scale vortices diminish and eventually disappear (Poggi et al. 2004b). Flexible canopies display a lower value,  $\beta = 0.17 \pm 0.01$  (Ghisalberti & Nepf 2005), consistent with the less efficient momentum transfer noted in **Figure 4**. Belcher et al. (2003) proposed the alternative  $K_u = (2\ell_m^2 L_c)^{-1/3}$ , with the approximation  $\ell_m \sim b$ . However, the mixing length within the canopy may be better represented by the vortex penetration, i.e.,  $\ell_m \sim L_c \sim (C_D a)^{-1}$ , which then also yields  $K_u \sim L_c^{-1} \sim C_D a$ .

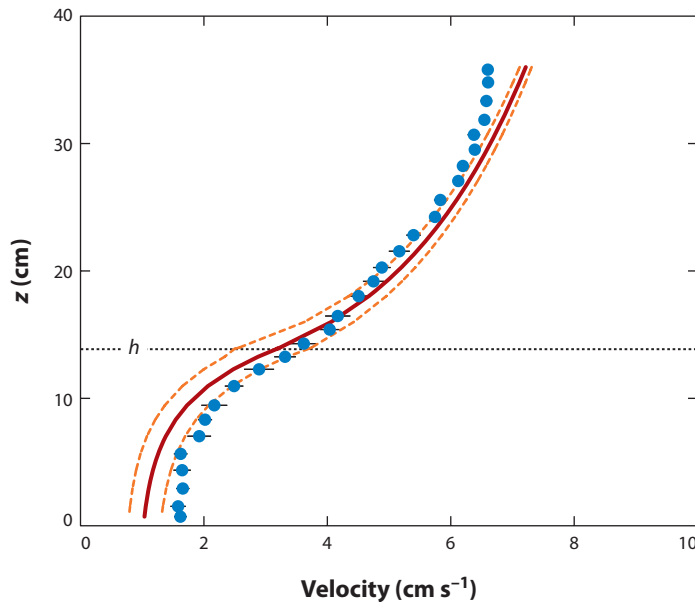


**Figure 5**

Measured velocity (*dots*) from Ghisalberti (2005). Predicted velocity (*solid line*) with confidence limits (*dashed lines*):  $H = 46.7$  cm,  $b = 13.9$  cm,  $S = 2.5 \times 10^{-5}$ ,  $a = 0.034$  cm $^{-1}$ , and  $C_D = 0.77$  (measured). Above the meadow, the velocity is predicted from the logarithmic profile (Equation 12), with  $u_* = [gS(H - b)]^{0.5}$ ,  $z_m = b - (1/2)\delta_z$  (Equation 13), and  $z_0 = (0.04 \pm 0.02)a^{-1}$ . Inside the meadow, the velocity is predicted from Equations 14 and 15, with  $U_b$  taken from logarithmic fit.

To model the full velocity profile, i.e., both within and above the bed, researchers have combined the models for above-canopy and in-canopy profiles by matching the velocity at the top of the canopy (e.g., Carollo et al. 2002, Abdelrhman 2003). Although this ignores the roughness sublayer, for practical purposes the resulting profile is reasonably accurate. First, the velocity profile above the meadow ( $z > b$ ) is estimated from the logarithmic profile (Equation 12). The logarithmic profile provides the velocity at the top of the meadow,  $U_b$ , which is used with Equations 14 and 15 to predict the velocity within the meadow ( $z < b$ ). An example is given in **Figure 5** using data from Ghisalberti (2005). The input parameters are the water depth ( $H = 46.7$  cm), the meadow height ( $b = 13.9$  cm), the surface slope ( $S = 2.5 \times 10^{-5}$ ), the canopy density ( $a = 0.034$  cm $^{-1}$ ), and the measured drag coefficient ( $C_D = 0.77$ ). The measured and predicted profiles agree within uncertainty except when approaching the free surface, where the measured profile tends toward  $\partial u / \partial z = 0$  to meet the no-stress condition at the surface that is not represented in the log profile. Other models for the complete velocity profile in regions with submerged aquatic vegetation have utilized different turbulence closure schemes (e.g., Shimizu & Tsujimoto 1994, Lopez & Garcia 2001, Poggi et al. 2004b, Defina & Bixio 2005), and some reflect the bending response of flexible vegetation (e.g., Abdelrhman 2007, Dijkstra & Uittenbogaard 2010).

## MASS TRANSPORT IN VEGETATED FLOW

Conservation of mass is described by the transport equation

$$\frac{\partial C}{\partial t} + \vec{u} \cdot \nabla C = D_m \nabla^2 C, \quad (16)$$



with  $D_m$  the molecular diffusion. Applying the double-averaging method described above, and assuming there are no sources or sinks, this becomes

$$\frac{\partial \langle \bar{C} \rangle}{\partial t} + \langle \bar{u}_j \rangle \frac{\partial \langle \bar{C} \rangle}{\partial x_j} = -\frac{1}{(1-\phi)} \frac{\partial}{\partial x_j} \left\{ (1-\phi) \left\{ \langle \bar{u}'_j \bar{C}' \rangle + \langle \bar{u}''_j \bar{C}'' \rangle - D_m \left\langle \frac{\partial \bar{C}}{\partial x_j} \right\rangle \right\} \right\}, \quad (17)$$

with  $(x, y, z) = (x_1, x_2, x_3)$ . The first term on the right-hand side represents the dispersion associated with turbulent fluctuations, i.e., turbulent diffusion. The second term on the right-hand side represents the dispersion associated with spatial heterogeneity in the time-mean velocity field, e.g., the dispersion associated with flow-path tortuosity. The last term is the flux due to molecular diffusion, which in general is negligible compared with the first two. Laboratory measurements in rigid canopies indicate that, over timescales greater than turbulent timescales, and spatial scales much greater  $\Delta S$  and  $d$ , these three terms produce Fickian transport; i.e., the right-hand side reduces to  $D_j(\partial^2 \langle \bar{C} \rangle / \partial x_j^2)$ , with  $D_j$  the dispersion coefficient (White & Nepf 2003, Tanino & Nepf 2008b).

### Turbulent Diffusion and Mechanical Dispersion in an Emergent Canopy

For solid volume fraction  $\phi < 0.1$ , turbulent diffusion is the dominant component of  $D$  within the canopy (Tanino & Nepf 2008b). The velocity scale controlling turbulent diffusion is the mean velocity,  $U_1$ , given by Equations 8 and 14. As discussed above, the turbulence length scale may be set by the stem scale (if  $d \leq S_n$ ) or by the stem spacing,  $S_n$ , for  $d > S_n$  (**Figure 2a**). Experimental studies confirm  $D \sim U_1 d$  for  $\phi \leq 0.1$  and support the simple scaling (Lightbody & Nepf 2006, Tanino & Nepf 2008b)

$$D = 0.2 U_1 d. \quad (18)$$

For denser canopies, specifically when  $S_n < d$ , the contribution to  $D$  from turbulent diffusion declines rapidly, as the length scale of turbulence declines (**Figure 2a**). For  $\phi \geq 0.1$ , the dispersion due to the spatial heterogeneity in the velocity field (also called mechanical dispersion) becomes important, and it dominates for  $\phi > 0.15$ . In addition, in the absence of turbulence, e.g.,  $Re_d < 100$ , mechanical dispersion is the main contributor to dispersion across all stem densities. The following formulation for mechanical dispersion is consistent with data across all stem densities for  $Re_d < 100$  and for  $\phi > 0.15$  for all Reynolds numbers (Nepf et al. 1997, Nepf 2004, Serra et al. 2004, Tanino & Nepf 2008b):

$$\frac{D}{U_1 d} = ad \approx \phi. \quad (19)$$

Tanino & Nepf (2008b) described a more comprehensive model that smoothly spans the two regimes described by Equations 18 and 19.

### Turbulent Diffusion Within and Above a Submerged Canopy

Because the canopy drag restricts the penetration of the canopy-scale vortices, a submerged canopy is segregated into two zones characterized by distinct turbulence scales. The canopy-scale vortices are excluded from the lower canopy ( $z < b - \delta_e$ ), and as a result the mechanisms of dispersion resemble those described above for emergent canopies. In contrast, transport in the upper canopy ( $z > b - \delta_e$ ) is dominated by canopy-scale turbulence so that the turbulent diffusivity scales on the size of the canopy-scale vortices and the velocity difference,  $\Delta U$ , between the canopy and the overflow, e.g., shown in **Figure 4**. The canopy-scale vortices grow to a size comparable to the shear-layer thickness  $t_{ml}$ . These scales also apply above a canopy with shallow submergence ( $H/b < 5$ ) because the canopy shear layer extends over most of the flow depth

(Ghisalberti & Nepf 2005, Ghisalberti & Nepf 2009). Based on experiments with rigid canopies,

$$D \approx 0.02 \Delta U t_{ml} \quad (20)$$

over the entire shear layer, i.e., both above and within the canopy (Ghisalberti & Nepf 2005, figure 11). Generally,  $t_{ml} \sim b$ , so Equation 20 can be estimated from the canopy height,  $b$ , and the velocity difference,  $\Delta U$ . The turbulent diffusivity has a peak at the top of the canopy, with  $D(z = b) \approx 0.032 \Delta U t_{ml}$ . As in a free shear layer, the turbulent diffusivity is higher than the turbulent viscosity ( $\nu_t$ ). The turbulent Schmidt number ( $S_t = \nu_t/D_t$ ) has a mean of 0.5 within the canopy shear layer, similar to other free shear layers, and a minimum of 0.3 at the top of the canopy, so that mass is mixed across the canopy-water interface three times more rapidly than is momentum (Ghisalberti & Nepf 2005, and references therein). For reference, in a neutral boundary layer  $S_t \approx 1$  (e.g., Kaimal & Finnigan 1994, p. 125). The lower value of  $S_t$  within a canopy shear layer can be explained by the numerical results discussed by Fitzmaurice et al. (2004). Ensemble averages of the velocity and pressure fields show that a region of high dynamic pressure is generated when a sweep encounters the canopy. While sweep events carry momentum and scalar downward via identical motions, the momentum transport is offset by high pressure generated at the canopy boundary, depressing the turbulent Schmidt number.

## SUMMARY

Aquatic vegetation significantly alters the mean and turbulent flow field. Within emergent canopies, the turbulent length scales are set by the stem diameter and spacing, and the mean flow is determined by the distribution of the canopy frontal area. Sparse submerged canopies ( $ab < 0.1$ ) enhance bed roughness and near-bed turbulence, but the velocity profile remains logarithmic. In contrast, dense submerged canopies ( $ab > 0.1$ ) transform the velocity profile to a mixing layer form. These canopies generate two distinct scales of turbulence: canopy-scale turbulence generated by flow instability at the top of the canopy and stem-scale turbulence generated within the canopy. Canopy-scale turbulence penetrates the canopy only over a length scale dependent on the canopy drag,  $\delta_e \sim (C_D a)^{-1}$ . This length scale determines both the displacement thickness ( $z_m$ ) for the logarithmic velocity profile above the canopy and the decay of stress-driven flow within the canopy. Furthermore,  $\delta_e$  separates a dense canopy into two regions of distinct transport. The upper canopy ( $z > b - \delta_e$ ) experiences energetic vertical transport and high levels of turbulent diffusion, controlled by canopy-scale vortices. The lower canopy ( $z < b - \delta_e$ ) experiences significantly slower transport, associated with the smaller element-scale turbulence.

## DISCLOSURE STATEMENT

The author is not aware of any biases that might be perceived as affecting the objectivity of this review.

## ACKNOWLEDGMENTS

The author is grateful for the insight and creativity of current and former students who contributed to this research, M. Ghisalberti, E. Murphy, B. White, A. Lightbody, Y. Tanino, M. Luhar, and J. Rominger, and especially for the editorial comments provided by M. Luhar and J. Rominger. Some of this material is based on work supported by the National Science Foundation under grants EAR 0309188, EAR 0125056, EAR 0738352, and OCE 0751358. Any opinions, conclusions, or recommendations expressed in this material are those of the author and do not necessarily reflect the views of the National Science Foundation.

## LITERATURE CITED

- Abdelrhman M. 2003. Effect of eelgrass *Zostera marina* canopies on flow and transport. *Mar. Ecol. Prog. Ser.* 248:67–83
- Abdelrhman M. 2007. Modeling coupling between eelgrass *Zostera marina* and water flow. *Mar. Ecol. Prog. Ser.* 338:81–96
- Ackerman JD. 1997. Submarine pollination in the marine angiosperm *Zostera marina*. *Am. J. Bot.* 84:1110–19
- Ackerman JD. 2000. Abiotic pollen and pollination: ecological, functional, and evolutionary perspectives. *Plant Syst. Evol.* 222:167–85
- Ackerman JD, Okubo A. 1993. Reduced mixing in a marine macrophyte canopy. *Funct. Ecol.* 7:305–9
- Alben S, Shelley M, Zhang J. 2002. Drag reduction through self-similar bending of a flexible body. *Nature* 420:479–81
- Anderson S, Charters A. 1982. A fluid dynamics study of seawater flow through *Gelidium nudifrons*. *Limnol. Oceanogr.* 27:399–412
- Belcher SE, Harman IN, Finnigan JJ. 2012. The wind in the willows: flows in forest canopies in complex terrain. *Annu. Rev. Fluid Mech.* 44:479–504
- Belcher S, Jerram N, Hunt J. 2003. Adjustment of a turbulent boundary layer to a canopy of roughness elements. *J. Fluid Mech.* 488:369–98
- Brampton AH. 1992. Engineering significance of British saltmarshes. In *Saltmarshes: Morphodynamics, Conservation, and Engineering Significance*, ed. JRL Allen, K Pye, pp. 115–22. Cambridge, UK: Cambridge Univ. Press
- Brown G, Roshko A. 1974. On density effects and large structure in turbulent mixing layers. *J. Fluid Mech.* 64:775–816
- Burke R, Stolzenbach K. 1983. Free surface flow through salt marsh grass. *MIT-Sea Grant Tech. Rep. MITSG 83-16*, Cambridge, MA
- Carollo F, Ferro V, Termini D. 2002. Flow velocity measurements in vegetated channels. *J. Hydraul. Eng.* 128:664–73
- Carpenter SR, Lodge DM. 1986. Effects of submersed macrophytes on ecosystem processes. *Aquat. Bot.* 26:341–70
- Chambers PA, Kalff J. 1985. Depth distribution and biomass of submersed aquatic macrophyte communities in relation to Secchi depth. *Can. J. Fish. Aquat. Sci.* 42:701–9
- Chandler M, Colarusso P, Buchsbaum R. 1996. A study of eelgrass beds in Boston Harbor and northern Massachusetts bays. *Proj. Rep., Off. Res. Dev., US EPA, Narragansett, RI*
- Cionco R. 1965. A mathematical model for air flow in a vegetation canopy. *J. Appl. Meteorol.* 4:517–22
- Coceal O, Belcher S. 2004. A canopy model of mean winds through urban areas. *Q. J. R. Meteorol. Soc.* 130:1349–72
- Costanza R, d'Arge R, de Groot R, Farber S, Grasso M, et al. 1997. The value of the world's ecosystem services and natural capital. *Nature* 387:253–60
- Defina A, Bixio A. 2005. Mean flow and turbulence in vegetated open channel flow. *Water. Resour. Res.* 41:W07006
- de Langre E. 2008. Effects of wind on plants. *Annu. Rev. Fluid Mech.* 40:141–68
- Dijkstra J, Uittenbogaard R. 2010. Modeling the interaction between flow and highly flexible aquatic vegetation. *Water. Resour. Res.* 46:W12547
- Dimotakis P, Debussy F, Koochesfahani M. 1981. Particle streak velocity field measurements in a two-dimensional mixing layer. *Phys. Fluids* 24:995–99
- Duarte CM. 1991. Seagrass depth limits. *Aquat. Bot.* 40:363–77
- Eckman J. 1990. A model of passive settlement by planktonic larvae onto bottoms of differing roughness. *Limnol. Oceanogr.* 35:887–901
- Finnigan J. 1979. Turbulence in waving wheat: I. Mean statistics and honami. *Bound.-Layer Meteorol.* 16:181–211
- Finnigan J. 2000. Turbulence in plant canopies. *Annu. Rev. Fluid Mech.* 32:519–71
- Finnigan J, Shaw R, Patton E. 2009. Turbulence structure above a vegetation canopy. *J. Fluid Mech.* 637:387–424

- Fitzmaurice L, Shaw RH, Paw U KT, Patton EG. 2004. Three-dimensional scalar microfront systems in a large-eddy simulation of vegetation canopy flow. *Bound.-Layer Meteorol.* 112:107–27
- Fonseca M, Kenworthy W. 1987. Effects of current on photosynthesis and distribution of seagrasses. *Aquat. Bot.* 27:59–78
- Furukawa K, Wolanski E, Mueller H. 1997. Currents and sediment transport in mangrove forests. *Estuar. Coast. Shelf Sci.* 44:301–10
- Gambi M, Nowell A, Jumars P. 1990. Flume observations on flow dynamics in *Zostera marina* (eelgrass) beds. *Mar. Ecol. Prog. Ser.* 61:159–69
- Gantzer C, Rittmann B, Herricks E. 1991. Effect of long-term water velocity changes on streambed biofilm activity. *Water Res.* 25:15–20
- Gao W, Shaw R, Paw U KT. 1989. Observation of organized structure in turbulent flow within and above a forest canopy. *Bound.-Layer Meteorol.* 47:349–77
- Gaylord B, Reed D, Washburn L, Raimondi P. 2004. Physical-biological coupling in spore dispersal of kelp forest macroalgae. *J. Mar. Syst.* 49:19–39
- Ghisalberti M. 2000. *Mixing layers and coherent structures in vegetated aquatic flows*. MS thesis. Mass. Inst. Technol. 126 pp.
- Ghisalberti M. 2005. *Momentum and scalar transport in vegetated shear flows*. PhD thesis. Mass. Inst. Technol. 119 pp.
- Ghisalberti M. 2009. Obstructed shear flows: similarities across systems and scales. *J. Fluid Mech.* 641:51–61
- Ghisalberti M, Nepf H. 2002. Mixing layers and coherent structures in vegetated aquatic flow. *J. Geophys. Res.* 107(C2):3011
- Ghisalberti M, Nepf H. 2004. The limited growth of vegetated shear layers. *Water Resour. Res.* 40:W07502
- Ghisalberti M, Nepf H. 2005. Mass transfer in vegetated shear flows. *Environ. Fluid Mech.* 5:527–51
- Ghisalberti M, Nepf H. 2006. The structure of the shear layer over rigid and flexible canopies. *Environ. Fluid Mech.* 6:277–301
- Ghisalberti M, Nepf H. 2009. Shallow flows over a permeable medium: the hydrodynamics of submerged aquatic canopies. *Transp. Porous Media* 78:385–402
- Gosselin F, de Langre E, Machado-Almeida B. 2010. Drag reduction of flexible plates by reconfiguration. *J. Fluid Mech.* 650:319–41
- Green EP, Short FT. 2003. *World Atlas of Seagrasses*. Berkeley: Univ. Calif. Press. 310 pp.
- Green J. 2005. Further comment on drag and reconfiguration of macrophytes. *Freshw. Biol.* 50:2162–66
- Gray WG, Lee PCY. 1977. On the theorems for local volume averaging of multiphase systems. *Int. J. Multiphase Flow* 3:333–40
- Grizzle R, Short F, Newell C, Hoven H, Kindblom L. 1996. Hydrodynamically induced synchronous waving of seagrasses: monami and its possible effects on larval mussel settlement. *J. Exp. Mar. Biol. Ecol.* 206:165–77
- Harman I, Finnigan J. 2007. A simple unified theory for flow in the canopy and roughness sublayer. *Bound.-Layer Meteorol.* 123:339–63
- Ho C-M, Zohar Y, Foss J, Buell J. 1991. Phase decorrelation of coherent structures in a free shear layer. *J. Fluid Mech.* 230:319–37
- Huang Y-H, Saiers J, Harvey J, Noe G, Mylon S. 2008. Advection, dispersion, and filtration of fine particles within emergent vegetation of the Florida Everglades. *Water. Resour. Res.* 44:W04408
- Hurd CL. 2000. Water motion, marine macroalgal physiology, and production. *J. Phycol.* 36:453–72
- Ikeda S, Kanazawa M. 1996. Three-dimensional organized vortices above flexible water plants. *J. Hydraul. Eng.* 122:634–40
- Inoue E. 1963. On the turbulent structure of airflow within crop canopies. *J. Meteorol. Soc. Jpn.* 49:121–24
- Jackson G, Winant C. 1983. Effect of a kelp forest on coastal currents. *Cont. Shelf Res.* 2:75–80
- Jarvela J. 2005. Effect of submerged flexible vegetation on flow structure and resistance. *J. Hydrol.* 307:233–41
- Jenter H, Duff M. 1999. Locally-forced wind effects on shallow waters with emergent vegetation. *Proc. 3rd Int. Symp. Ecohydraul., Salt Lake City, July 13–16*, CD-ROM. Madrid: IAHR
- Jimenez J. 2004. Turbulent flows over rough walls. *Annu. Rev. Fluid Mech.* 36:173–96
- Kaimal J, Finnigan J. 1994. *Atmospheric Boundary Layer Flows: Their Structure and Measurement*. New York: Oxford Univ. Press. 289 pp.

- Koch EW. 1994. Hydrodynamics, diffusion-boundary layers and photosynthesis of the seagrasses, *Thalassia testudinum* and *Cymodocea nodosa*. *Mar. Biol.* 118:767–76
- Leonard L, Croft A. 2006. The effect of standing biomass on flow velocity and turbulence in *Spartina alterniflora* canopies. *Coast. Shelf Sci.* 69:325–36
- Leonard L, Luther M. 1995. Flow hydrodynamics in tidal marsh canopies. *Limnol. Oceanogr.* 40:1474–84
- Leonard L, Reed D. 2002. Hydrodynamics and sediment transport through tidal marsh canopies. *J. Coast. Res.* 36:459–69
- Lightbody A, Nepf H. 2006. Prediction of velocity profiles and longitudinal dispersion in emergent salt marsh vegetation. *Limnol. Oceanogr.* 51:218–28
- Lopez F, Garcia M. 1998. Open-channel flow through simulated vegetation: suspended sediment transport modeling. *Water Resour. Res.* 34:2341–52
- Lopez F, Garcia M. 2001. Mean flow and turbulence structure of open-channel flow through non-emergent vegetation. *J. Hydraul. Res.* 127:392–402
- Lowe R, Koseff J, Monismith S. 2005. Oscillatory flow through submerged canopies: 1. Velocity structure. *J. Geophys. Res.* 110:C10016
- Lowe R, Shavit U, Falter J, Koseff J, Monismith S. 2008. Modeling flow in coral communities with and without waves: a synthesis of porous media and canopy flow approaches. *Limnol. Oceanogr.* 53:2668–80
- Luhar M, Coutu S, Infantes E, Fox S, Nepf H. 2010. Wave induced velocities inside a model seagrass bed. *J. Geophys. Res.* 115:C12005
- Luhar M, Rominger J, Nepf H. 2008. Interaction between flow, transport and vegetation spatial structure. *Environ. Fluid Mech.* 8:423–39
- Macdonald R, Griffiths R, Hall D. 1998. An improved method for the estimation of surface roughness of obstacle arrays. *Atmos. Environ.* 32:1857–64
- Mazda Y, Wolanski E, King B, Sase A, Ohtsuka D, Magi M. 1997. Drag forces due to vegetation in mangrove swamps. *Mangroves Salt Marshes* 1:193–99
- Mitsch WJ, Gosselink JG. 1986. *Wetlands*. New York: Van Nostrand Reinhold. 712 pp. 2nd ed.
- Monismith S. 2007. Hydrodynamics of corals. *Annu. Rev. Fluid Mech.* 39:37–55
- Moore KA. 2004. Influence of seagrasses on water quality in shallow regions of the lower Chesapeake Bay. *J. Coast. Res.* 20:162–78
- Murphy E, Ghisalberti M, Nepf H. 2007. Model and laboratory study of dispersion in flows with submerged vegetation. *Water Resour. Res.* 43:W05438
- Naden P, Rameshwaran P, Mountford O, Robertson C. 2006. The influence of macrophyte growth, typical of eutrophic conditions, on river flow velocities and turbulence production. *Hydrol. Process.* 20:3915–38
- Nepf H. 1999. Drag, turbulence, and diffusion in flow through emergent vegetation. *Water Resour. Res.* 35:479–89
- Nepf H. 2004. Vegetated flow dynamics. In *Ecogeomorphology of Tidal Marshes*, ed. S Fagherazzi, M Marani, L Blum, pp. 137–63. *Coast. Estuar. Monogr. Ser.* Washington, DC: Am. Geophys. Union
- Nepf H. 2012. Flow over and through biota. In *Treatise on Estuarine and Coastal Science*, ed. E Wolanski, D McLusky. San Diego: Elsevier. In press
- Nepf H, Ghisalberti M, White B, Murphy E. 2007. Retention time and dispersion associated with submerged aquatic canopies. *Water Resour. Res.* 43:W04422
- Nepf H, Koch E. 1999. Vertical secondary flows in submersed plant-like arrays. *Limnol. Oceanogr.* 44:1072–80
- Nepf H, Sullivan J, Zavistoski R. 1997. A model for diffusion within an emergent plant canopy. *Limnol. Oceanogr.* 42:85–95
- Nepf H, Vivoni E. 2000. Flow structure in depth-limited, vegetated flow. *J. Geophys. Res.* 105:547–57
- Nikora N, Nikora V. 2007. A viscous drag concept for flow resistance in vegetated channels. *Proc. 32nd IAHR Congr., Venice, 1–6 July*, CD-ROM. Madrid: IAHR
- O'Hare M, Hutchinson K, Clarke R. 2007. The drag and reconfiguration experienced by five macrophytes from a lowland river. *Aquat. Bot.* 86:253–59
- Okamoto T, Nezu I. 2009. Turbulence structure and monami phenomena in flexible vegetated open-channel flows. *J. Hydraul. Res.* 47:798–810
- Oldham C, Sturman J. 2001. The effect of emergent vegetation on convective flushing in shallow wetlands. *Limnol. Oceanogr.* 46:1486–93

- Poggi D, Katul G, Albertson J. 2004a. A note on the contribution of dispersive fluxes to momentum transfer within canopies. *Bound.-Layer Meteorol.* 111:615–21
- Poggi D, Porporato A, Ridolfi L, Albertson J, Katul G. 2004b. The effect of vegetation density on canopy sub-layer turbulence. *Bound.-Layer Meteorol.* 111:565–87
- Raupach M, Finnigan J, Brunet Y. 1996. Coherent eddies and turbulence in vegetation canopies: the mixing-layer analogy. *Bound.-Layer Meteorol.* 60:375–95
- Raupach M, Shaw R. 1982. Averaging procedures for flow within vegetation canopies. *Bound.-Layer Meteorol.* 22:79–90
- Raupach M, Thom A, Edwards I. 1980. A wind-tunnel study of turbulent flow close to regularly arrayed rough surfaces. *Bound.-Layer Meteorol.* 18:373–97
- Rominger J, Nepf H. 2011. Flow adjustment and interior flow associated with a rectangular porous obstruction. *J. Fluid Mech.* 680:636–59
- Sand-Jensen K. 2003. Drag and reconfiguration of freshwater macrophytes. *Freshw. Biol.* 48:271–83
- Sand-Jensen K. 2008. Drag forces on common plant species in temperate streams: consequences of morphology, velocity, and biomass. *Hydrobiologia* 610:307–19
- Serra T, Fernando HJS, Rodriquez R. 2004. Effects of emergent vegetation on lateral diffusion in wetlands. *Water Res.* 38:139–47
- Shimizu Y, Tsujimoto T. 1994. Numerical analysis of turbulent open-channel flow over a vegetation layer using a  $k-\epsilon$  turbulence model. *J. Hydroscl. Hydraul. Eng.* 11:57–67
- Statzner B, Lamouroux N, Nikora V, Sagnes P. 2006. The debate about drag and reconfiguration of freshwater macrophytes: comparing results obtained by three recently discussed approaches. *Freshw. Biol.* 51:2173–83
- Sukhodolov A. 2005. Comment on drag and reconfiguration of macrophytes. *Freshw. Biol.* 50:194–95
- Tanino Y, Nepf H. 2008a. Laboratory investigation on mean drag in a random array of rigid, emergent cylinders. *J. Hydraul. Eng.* 134:34–41
- Tanino Y, Nepf H. 2008b. Lateral dispersion in random cylinder arrays at high Reynolds number. *J. Fluid Mech.* 600:339–71
- Tanino Y, Nepf H, Kulis P. 2005. Gravity currents in aquatic canopies. *Water Resour. Res.* 41:W12402
- Tennekes H, Lumley J. 1972. *A First Course in Turbulence*. Cambridge, MA: MIT Press. 300 pp.
- Thom A. 1971. Momentum absorption by vegetation. *Q. J. R. Meteorol. Soc.* 97:414–28
- Valiela I, Teal J, Deuser W. 1978. The nature of growth forms in the salt marsh grass *Spartina alterniflora*. *Am. Nat.* 112:461–70
- van Katwijk M, Bos A, Hermus D, Suykerbuyk W. 2010. Sediment modification by seagrass beds: muddification and sandification induced by plant cover and environmental conditions. *Estuar. Coast. Shelf Sci.* 89:175–81
- Vogel S. 1994. *Life in Moving Fluid*. Princeton, NJ: Princeton Univ. Press. 484 pp. 2nd ed.
- Whitaker S. 1996. The Forchheimer equation: a theoretical development. *Trans. Porous Media* 25:27–61
- White B, Nepf H. 2003. Scalar transport in random cylinder arrays at moderate Reynolds number. *J. Fluid Mech.* 487:43–79
- White B, Nepf H. 2007. Shear instability and coherent structures in a flow adjacent to a porous layer. *J. Fluid Mech.* 593:1–32
- Winant C, Browand F. 1974. Vortex pairing: the mechanism of turbulent mixing-layer growth at moderate Reynolds number. *J. Fluid Mech.* 63:237–55
- Wooding R, Bradley E, Marshall J. 1973. Drag due to regular arrays of roughness elements. *Bound.-Layer Meteorol.* 5:285–308





# Contents

Aeroacoustics of Musical Instruments <i>Benoit Fabre, Joël Gilbert, Avraham Hirschberg, and Xavier Pelorson</i> .....	1
Cascades in Wall-Bounded Turbulence <i>Javier Jiménez</i> .....	27
Large-Eddy-Simulation Tools for Multiphase Flows <i>Rodney O. Fox</i> .....	47
Hydrodynamic Techniques to Enhance Membrane Filtration <i>Michel Y. Jaffrin</i> .....	77
Wake-Induced Oscillatory Paths of Bodies Freely Rising or Falling in Fluids <i>Patricia Ern, Frédéric Risso, David Fabre, and Jacques Magnaudet</i> .....	97
Flow and Transport in Regions with Aquatic Vegetation <i>Heidi M. Nepf</i> .....	123
Electrorheological Fluids: Mechanisms, Dynamics, and Microfluidics Applications <i>Ping Sheng and Weijia Wen</i> .....	143
The Gyrokinetic Description of Microturbulence in Magnetized Plasmas <i>John A. Krommes</i> .....	175
The Significance of Simple Invariant Solutions in Turbulent Flows <i>Genta Kawahara, Markus Uhlmann, and Lennaert van Veen</i> .....	203
Modern Challenges Facing Turbomachinery Aeroacoustics <i>Nigel Peake and Anthony B. Parry</i> .....	227
Liquid Rope Coiling <i>Neil M. Ribe, Mehdi Habibi, and Daniel Bonn</i> .....	249
Dynamics of the Tear Film <i>Richard J. Braun</i> .....	267
Physics and Computation of Aero-Optics <i>Meng Wang, Ali Mani, and Stanislav Gordeyev</i> .....	299

Smoothed Particle Hydrodynamics and Its Diverse Applications <i>J. J. Monaghan</i> .....	323
Fluid Mechanics of the Eye <i>Jennifer H. Siggers and C. Ross Ethier</i> .....	347
Fluid Mechanics of Planktonic Microorganisms <i>Jeffrey S. Guasto, Roberto Rusconi, and Roman Stocker</i> .....	373
Nanoscale Electrokinetics and Microvortices: How Microhydrodynamics Affects Nanofluidic Ion Flux <i>Hsueh-Chia Chang, Gilad Yossifon, and Evgeny A. Demekhin</i> .....	401
Two-Dimensional Turbulence <i>Guido Boffetta and Robert E. Ecke</i> .....	427
“Vegetable Dynamicks”: The Role of Water in Plant Movements <i>Jacques Dumais and Yoël Forterre</i> .....	453
The Wind in the Willows: Flows in Forest Canopies in Complex Terrain <i>Stephen E. Belcher, Ian N. Harman, and John J. Finnigan</i> .....	479
Multidisciplinary Optimization with Applications to Sonic-Boom Minimization <i>Juan J. Alonso and Michael R. Colonno</i> .....	505
Direct Numerical Simulation on the Receptivity, Instability, and Transition of Hypersonic Boundary Layers <i>Xiaolin Zhong and Xiaowen Wang</i> .....	527
Air-Entrainment Mechanisms in Plunging Jets and Breaking Waves <i>Kenneth T. Kiger and James H. Duncan</i> .....	563

## Indexes

Cumulative Index of Contributing Authors, Volumes 1–44 .....	597
Cumulative Index of Chapter Titles, Volumes 1–44 .....	606

## Errata

An online log of corrections to *Annual Review of Fluid Mechanics* articles may be found at <http://fluid.annualreviews.org/errata.shtml>